Optical and structural study of the pressure-induced phase transition of $CdWO_4$

J. Ruiz-Fuertes,[1,*] A. Friedrich,[2,3] D. Errandonea,[1] A. Segura,[1] W. Morgenroth,[2] P. Rodríguez-Hernández,[4] A. Muñoz,[4] and Y. Meng[5]

[1]*MALTA-Consolider Team. Departament de Física Aplicada-ICMUV, Universitat de València, Dr. Moliner 50, 46100 Burjassot, Valencia, Spain*
[2]*Institut für Geowissenschaften, Goethe-Universität Frankfurt, Altenhöferallee 1, 60438 Frankfurt am Main, Germany*
[3]*Institut für Anorganische Chemie, Julius-Maximilians-Universität Würzburg, Am Hubland, 97074 Würzburg, Germany*
[4]*Instituto de Materiales y Nanotecnología, Departamento de Física, Universidad de La Laguna, La Laguna, 38205 Tenerife, Spain*
[5]*HPCAT, Carnegie Institution of Washington, Bldg. 434E, 9700 S. Cass Avenue, Argonne, IL 60439, USA*

(Dated: April 11, 2017)

The optical absorption of $CdWO_4$ is reported at high pressures up to 23 GPa. The onset of a phase transition was detected at 19.5 GPa, in good agreement with a previous Raman spectroscopy study. The crystal structure of the high-pressure phase of $CdWO_4$ was solved at 22 GPa employing single-crystal synchrotron x-ray diffraction. The symmetry changes from space group $P2/c$ in the low-pressure wolframite phase to $P2_1/c$ in the high-pressure post-wolframite phase accompanied by a doubling of the unit-cell volume. The octahedral oxygen coordination of the tungsten and cadmium ions is increased to [7]-fold and [6+1]-fold, respectively, at the phase transition. The compressibility of the low-pressure phase of $CdWO_4$ has been reevaluated with powder x-ray diffraction up to 15 GPa finding a bulk modulus of B_0 = 123 GPa. The direct bandgap of the low-pressure phase increases with compression up to 16.9 GPa at 12 meV/GPa. At this point an indirect bandgap crosses the direct bandgap and decreases at -2 meV/GPa up to 19.5 GPa where the phase transition starts. At the phase transition the bandgap collapses by 0.7 eV and another direct bandgap decreases at -50 meV/GPa up to the maximum measured pressure. The structural stability of the post-wolframite structure is confirmed by *ab initio* calculations finding the post-wolframite-type phase to be more stable than the wolframite at 18 GPa. Lattice dynamic calculations based on space group $P2_1/c$ explain well the Raman-active modes previously measured in the high-pressure post-wolframite phase. The pressure-induced bandgap crossing in the wolframite phase as well as the pressure dependence of the direct bandgap in the high-pressure phase are further discussed with respect to the calculations.

I. INTRODUCTION

Nowadays used as a scintillating detector in x-ray tomography[1], high-energy particle physics[2], and dosimetry devices[3], the wide-bandgap (4 eV) semiconductor cadmium tungstate ($CdWO_4$) has been extensively studied during the last three decades. It possesses a high light yield emission when hit by γ particles or x-rays and despite its long scintillation time (12-15 μs)[4], it played a key role in the discovery[5] of the natural alpha activity in ^{180}W. Also, the long decay time of the radiation created by self-trapped Frenkel excitons of $CdWO_4$ makes this material a test bench for studying exciton-exciton interactions in semiconductors[6]. In order to improve the versatility of $CdWO_4$ as a scintillating material, understanding how doping[7] or externally modifying its interatomic distances affect its electronic structure, are of interest. In this context, pressure is an efficient tool to correlate changes in the bond distances with electronic properties.

$CdWO_4$ crystallizes in a wolframite-type structure (space group $P2/c$) at ambient conditions in which both Cd and W atoms are octahedrally coordinated (Fig. 1). Such a structure confers $CdWO_4$ a direct bandgap along the Z direction of the Brillouin zone[8–10]. At high pressures, the conduction band, mainly contributed by the $5d$ W levels, moves up as a result of the increase of repulsion, giving rise to a widening of the band gap at 12(1) meV/GPa up to at least 9.9 GPa[10]. Previous high-pressure polarized optical microscopic studies[11] showed the emergence of aligned color domains at around 10 GPa in $CdWO_4$, probably due to the low-hydrostatic conditions. However, high-pressure Raman spectroscopy studies revealed that $CdWO_4$ remains in the wolframite-type structure up to at least 20 GPa[11,12]. Above this pressure the number of Raman-active modes abruptly increases as a consequence of a phase transition, interpreted by the coexistence of a triclinic $CuWO_4$-type structure and a tetragonal scheelite-type structure, according to the predictions[12]. The proposed formation and coexistence of the two energetically similarly stable high-pressure phases at the same pressure, though explained the number of the observed Raman modes, is controversial since those Raman spectroscopy experiments were performed using a single crystal[12]. In order to study such a phase transition one should employ a structural technique on a single crystal at the same experimental conditions. However, previous single-crystal x-ray diffraction (SXRD) has been limited to 8.2 GPa[13]. Furthermore, previous electronic band structure calculations have indicated a band crossing in $CdWO_4$ at 16 GPa, a pressure not experimentally explored yet[10] with optical absorption.

In this work we present a powder XRD and a SXRD study of $CdWO_4$ up to 15 GPa and 22 GPa, respectively, to solve the structure of its high-pressure phase, and an optical absorption study up to 23 GPa to investigate the effect that the structural phase transition has on the optical properties of $CdWO_4$. Finally, the stability of the high-pressure phase of $CdWO_4$, the frequencies of its Raman modes, and its electronic properties

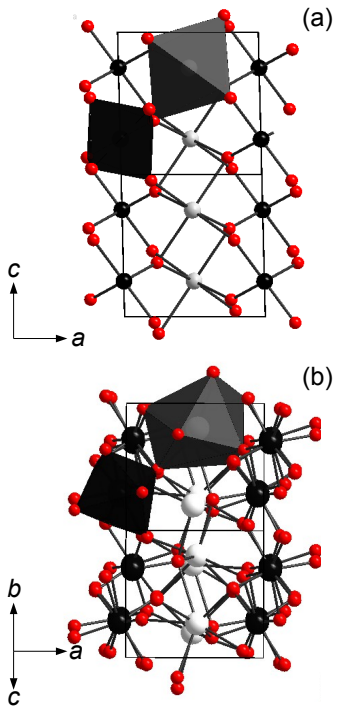

FIG. 1: Projections along (a) the [010] direction of the wolframite and (b) [011] direction of the post-wolframite-type structures of $CdWO_4$. The large white and black spheres represent the Cd and W atoms, respectively. The small spheres are the O atoms.

have been investigated using *ab initio* calculations.

II. EXPERIMENTAL DETAILS

For the non polarized optical absorption experiments at high pressure two 10-μm-thick samples of $CdWO_4$ were cleaved along the (010) plane from a large single crystal obtained from the MTI Corporation. In this orientation the cross-polarization terms of the complex reflection are both zero[14]. The samples were loaded in Neon pressure medium together with a ruby chip for pressure calibration[15] in a membrane-type diamond anvil cell (DAC) with 500-μm culet anvils. The pressure chamber consisted of a hole with a diameter of 200-μm drilled in an Inconel gasket previously preindented to 45-μm thickness. The confocal optical setup used for the measurements consisted in a deuterium-halogen lamp, fused silica lenses, two Cassegrain objectives, and an UV-VIS spectrometer. The powder XRD experiments were carried out up to 15 GPa at the 16-IDB beamline of the HPCAT at the Advanced Photon Source (APS). The experiment was performed in a symmetric DAC with 480-μm diamond culets and a rhenium gasket with a hole of 150 μm was used as the pressure chamber. Neon was employed as pressure medium and the ruby fluorescence was used for pressure calibration. The monochromatic x-ray beam used had a wavelength of λ= 0.36783 Å and was focused down to 10×10 μm^2. For the SXRD experiments we loaded a single-crystal sample together with a ruby chip and Neon was used as pressure medium in Boehler-Almax DACs equipped with diamond culets of 350 μm diameter and tungsten gaskets preindented to 45 μm thickness with a hole of 160-μm diameter. The experiments were carried out at 15 and 22 GPa at the Extreme Conditions Beamline at PETRA III (λ = 0.2925 Å and 0.2904 Å, respectively) using a PerkinElmer 1621 detector with a 8.3×9.6 μm^2 and 4×8 μm^2 beam and a sample to detector distance of 402.5 mm and 430.6 mm, respectively. The diffraction images were collected by 1° ω-scanning. The image format was converted according to the procedure described by Rothkirch et al.[16] for further processing with the CrysAlisPro software[17] for indexing reflections and intensity data reduction. The crystal structure of the high-pressure phase of $CdWO_4$ exhibits a pseudo-orthorhombic metric at 22 GPa. However, attempts to solve the crystal structure in an orthorhombic space group were unsuccessful. Finally, the crystal structure was successfully solved in space group Pc with SHELXS97-2[18] using direct methods and was subsequently converted to space group $P2_1/c$ using PLATON[19]. A pseudo-merohedral 2-component twin (55 %) related via a twin plane perpendicular to the c-axis with the twin matrix (1 0 0, 0 1 0, 0 0 -1) was refined with SHELXL97-2[18]. The programs were used with the WinGX interface[20]. The final refinements were carried out with anisotropic displacement parameters for the tungsten and cadmium atoms and isotropic ones for the oxygen atoms. The final residual value R1 of the post-wolframite structure converged to 6.34 % at a data:parameter ratio of $\approx$ 26, which are excellent values for single-crystal structure refinements of high-pressure data, and even more for a twinned high-pressure phase.

III. COMPUTATIONAL DETAILS

First principles calculations of the total-energy to study electronic structure and lattice dynamics were done within the framework of the density-functional theory (DFT)[21] and the pseudo-potential method using the Vienna *ab initio* simulation package (VASP)[22–24]. The exchange and correlation energy were used in the generalized gradient approximation (GGA) with the PBE functional[25]. The projector-augmented wave (PAW) scheme[26,27] was adopted and the semicore $5p$ W electrons were also explicitly included in the calculations. The considered valence electron configuration was Cd $4d^{10}5s^2$, O $2s^22p^4$, and W $5d^46s^2$. The set of plane waves employed extended up to the kinetic energy cutoff of 530 eV to deal with the O atoms in order to have highly accurate results. The Monkhorst-Pack[28] grid used for Brillouin-zone integrations ensured converged results to about 1 meV per formula unit. To perform the geometrical optimization we used 20 special k-points of the reciprocal space with symmetry $P2/c$, 14 k-points with $P2_1/c$, and 36 and 39 k-points for P_1 and $I4_1/a$ symmetries, respectively. In our simulations we obtain not only the energy and volume, we also obtain derivatives of the energy, forces, and stres. Hence, we also obtain the pressure from the *ab initio* simulations. In fact when we relax for a volume a structure, the relaxed structure should have diagonal

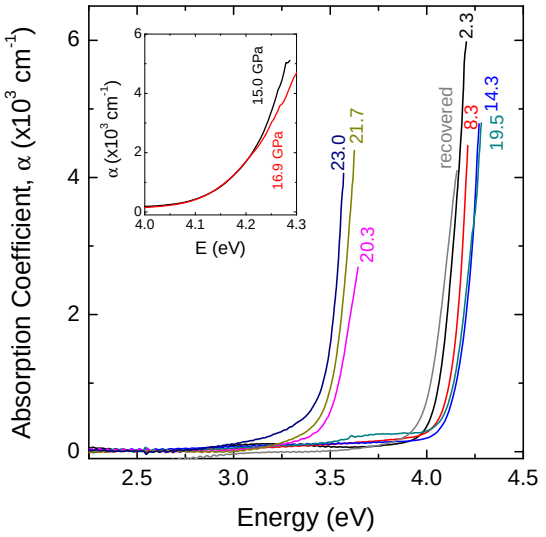

FIG. 2: Optical absorption spectra of $CdWO_4$ at different pressures up to 23 GPa. The inset shows the change of the shape of the absorption edge at 16.9 GPa compared to the spectrum at 15.0 GPa.

stress tensor (hydrostatic), and zero forces on the atoms. In the relaxed equilibrium configuration the forces on the atoms were lower than 0.002 eV/Å and the deviation of the stress tensor from a diagonal hydrostatic form was less than 0.1 GPa. Lattice dynamic calculations were carried out at Γ using the direct forces constant approach. This method involves the construction of the dynamical matrix, that requires highly converged results on forces. Diagonalization of the dynamical matrix provides both the frequencies of the normal modes and their polarization vectors. This allows us to identify the irreducible representation and the character of the phonon modes at the zone center. More details of the calculations can be found in Refs.[10,12,29]

IV. EXPERIMENTAL RESULTS

A. Optical Absorption

A selection of absorption-coefficient (α) spectra of $CdWO_4$ at different pressures can be found in Fig. 2. At ambient pressure the absorption edge shows a steep increase up to a maximum value of $\alpha \approx 6{\times}10^3$ cm^{-1}, in good agreement with a direct band gap[10]. As observed in previous results up to 10 GPa[10], as pressure increases, the absorption edge keeps the same shape and shifts from 4 eV to higher energies up to 15 GPa. At 16.9 GPa the absorption edge reduces its steepness and starts to downshift to lower energies with increasing pressure up to 19.5 GPa when the sample exhibits a subtle color change and a low-absorbance step-like absorption spectrum emerges at lower energy ($\approx$ 3.5 eV) in coexistence with the main absorption edge (Fig. 2). The shape of the newly emerged absorption spectrum indicates the contribution of two distinct electronic transitions with different absorbances. $CdWO_4$ undergoes a structural phase transition at 20 GPa according to Raman Spectroscopy[12]. Therefore, the existence of an additional low-absorbance absorption edge at 19.5 GPa can be attributed to the onset of the phase transition to the high-pressure phase, which at this pressure is a minor component. This is confirmed at 20.3 GPa with the loss of the high-energy absorption edge and an abrupt increase in the absorpbance of the low-energy absorption edge ($\alpha \approx 4{\times}10^3$ cm^{-1}), indicating the end of the phase transition. At higher pressures the absorption edge of the high-pressure phase of $CdWO_4$ decreases in energy with further compression.

The steep-shaped absorption edges observed in the low-pressure phase absorption edge up to 15 GPa and in the high-pressure phase above 20.3 GPa are typical of direct bandgaps. We have analyzed the absorption spectra in both phases employing the direct-bandgap Urbarch's rule $\alpha = A_0 \cdot \exp[(h\nu - E_g)/E_U]$, where E_g is the bandgap, E_U is Urbach's energy and is related to the steepness of the absorption tail, and A_0 is an intrinsic constant of the sample that accounts for the absorption of defects[30]. The fits to spectra of the low- and high-pressure phases (Fig. 3) confirm the direct nature of the bandgaps in both phases (except at 16.9 and 19.5 GPa). In hydrostatic conditions[31], where uniaxial stresses do not deteriorate the sample, E_U and A_0 can be assumed to remain constant under pressure as long as the structure of the compounds and the density of defects remain constant[32]. In the case of $CdWO_4$ we have obtained an A_0 value of 600 cm^{-1} for both phases in good agreement with other wolframite-type compounds ($A_0 = 500$ cm^{-1} for $MgWO_4$)[10]. For the E_U, it takes a value of 0.056 eV in the low-pressure phase and 0.082 eV in the high-pressure phase. The higher value observed for E_U in the high-pressure phase indicates an increase of point defects usually observed after a structural phase transition[33–35]. Regarding the absorption edges at 16.9 GPa and 19.5 GPa, in Fig. 2 we can see that they lose steepness, redshift with pressure, and cross the absorption edges measured at lower pressures. The linear dependence of $\alpha^{1/2}$ with the photon energy (Fig. 3) confirms the indirect nature of the bandgap at 16.9 and 19.5 GPa. After releasing pressure the recovered sample shows an absorption edge recovers the shape and energy of the measured spectra on pressure increase for the low-pressure phase. This confirms the reversibility of the phase transition and the fact that pressure apparently does not induce defects in the used hydrostatic conditions.

The values of the bandgap energy obtained from the analysis of all measured spectra are shown in Fig. 4 together with the data from Ref.[10]. We show that in the wolframite-type phase, the bandgap increases up to 15 GPa with a pressure coefficient dE_g/dp of 12 meV/GPa in good agreement with previous data[10]. Above 15 GPa, the change from a direct to an indirect bandgap, associated to a band crossing previously reported[10] and observed in other wolframites before the phase transition[36], implies a negative pressure coefficient of -2 meV/GPa. At the phase transition the bandgap collapses by 0.7 eV, with the direct bandgap of the high-pressure phase showing a negative pressure dependence of -50 meV/GPa.

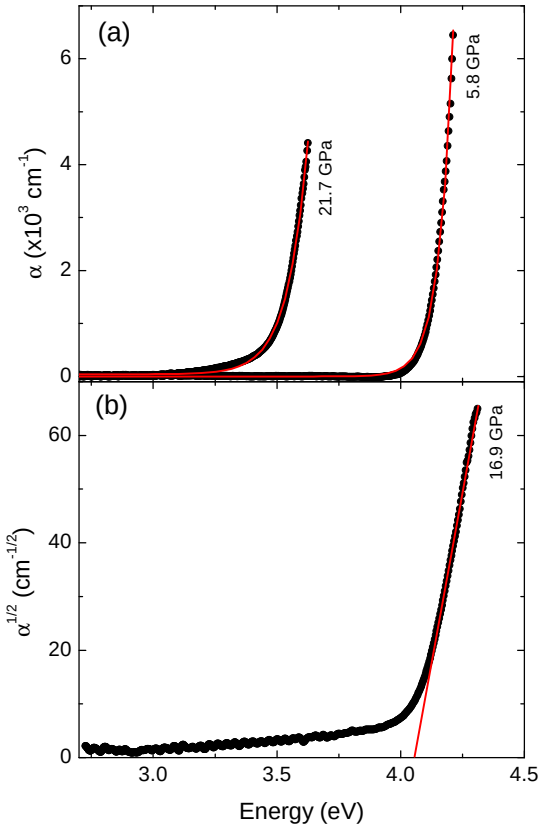

FIG. 3: (a) Fits to the Urbach's rule (red line) to two spectra at 5.8 and 21.7 GPa (black points) that correspond to the low-pressure and high-pressure phases of $CdWO_4$, respectively. (b) Linear dependence of $\alpha^{1/2}$ of the spectrum at 16.9 GPa showing the indirect nature of the bandgap at this pressure.

B. X-ray diffraction

As explained in Sec. II, we carried out one powder XRD experiment up to 15 GPa and two SXRD experiments with $CdWO_4$. One of the two SXRD experiments was performed below and the other one above the phase transition at 15 GPa and 22 GPa, respectively. The powder diffraction patterns of $CdWO_4$ at 1.3 and 13.2 GPa are shown as supporting information.

The unit-cell parameters and atomic coordinates obtained from the structural refinements of the single crystals at those two pressures are given in table I. A detailed table with the data collection parameters and refinement results including the equivalent or isotropic displacement parameters at 15 GPa for the low-pressure wolframite-type phase and at 22 GPa for the high-pressure post-wolframite phase has been deposited as supporting information.

In Fig. 5 we show the pressure dependence of the unit-cell volume and lattice parameters from a previous study by Macavei and Schulz [13] and from our powder XRD and SXRD experiments. Previous SXRD data[13] had been limited to 8.2 GPa. We have increased the pressure range to 15 GPa for the low-pressure phase and observed that the bulk modulus of

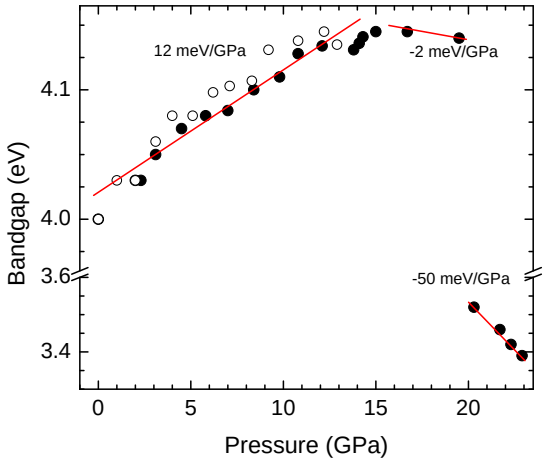

FIG. 4: Pressure dependence of the bandgap energy of $CdWO_4$. Open circles represent data from Ref.[10] while filled circles are from data collected in this study. The continuous red lines show the fits.

this phase[13] had been overestimated (Fig. 5a). Using a second order Birch-Murnaghan equation of state to fit the combined data of Macavei and Schulz [13] and ours, we obtain a bulk modulus $B_0 = 123$ GPa instead of 136 GPa that had previously been reported by Macavei and Schulz [13]. Regarding the lattice parameters (Fig. 5b) we confirm the observation by Macavei and Schulz [13] that the b axis is more compressible than the other axes. Similarly to $MnWO_4$[37], the β monoclinic angle increases with pressure up to the phase transition.

The crystal structure of the high-pressure post-wolframite phase of $CdWO_4$ was solved at 22 GPa from the SXRD data. While the a-axis is increased with respect to the low-pressure structure at 15 GPa, the **b** and **c** basis vectors of the post-wolframite cell relate to the diagonal directions $[0\bar{1}1]$ and $[0\bar{1}\bar{1}]$ in the **bc** plane of the wolframite cell, respectively. This is also reflected in a doubling of the unit cell volume of the post-wolframite phase with respect to that of the wolframite phase, and hence of the formula units from 2 to 4. The transformation can be described by the transformation matrix [1 0 0, 0 -1 1, 0 -1 -1]. The space group symmetry changes from $P2/c$ in the wolframite phase to $P2_1/c$ in the post-wolframite phase ($\vec{b'}$ = -$\vec{b}$+$\vec{c}$, $\vec{c'}$=-$\vec{b}$-$\vec{c}$) at the phase transition accompanied by a change in the monoclinic b-axis direction. The orientation relation between the wolframite and the post-wolframite phase was confirmed by a comparison of the orientation matrices of the same crystal at pressures below and above the phase transition. There is no group-subgroup relationship between the wolframite ($P2/c$) and post-wolframite ($P2_1/c$) space groups. A comparison of half of the post-wolframite unit-cell volume at 22 GPa with the wolframite unit-cell volume extrapolated from the equation of state to 22 GPa indicates a volume reduction of about 8 % at the phase transition (Fig. 5a). Such a huge volume drop points towards a first-order type of phase transition. Most of the volume compression is achieved by the compression of the wolframite b axis, which also compensates for the significant increase of the a axis (Fig. 5b). The crystal structure is severely reor-

TABLE I: Lattice parameters, atomic coordinates, and equivalent or isotropic displacement parameters, respectively, of the experimental and calculated wolframite-type and post-wolframite-type structures of $CdWO_4$. The lattice parameters are in Å, the β angle is in degrees, the unit-cell volume is in $Å^3$, and the displacement parameters are in $Å^2$.

		$P2/c$		$P2_1/c$	
		15 GPa	16 GPa	22 GPa	22.9 GPa
		Exp.	**Calc.**	**Exp.**	**Calc.**
	a	4.9431(4)	4.9795	5.1884(7)	5.2585
	b	5.498(5)	5.6553	6.1898(17)	6.2535
	c	4.9685(4)	5.0110	7.5402(17)	7.66382
	β	93.136(6)	92.26	90.01(2)	90.67
	V	134.82(12)	140.99	242.15(9)	251.99
	Z	2	2	4	4
Cd	x	0.5	0.5	0.5162(3)	0.51039
	y	0.7126(1)	0.70415	0.7675(3)	0.76775
	z	0.25	0.25	-0.0358(2)	-0.02630
	U_{eq}	0.007(2)		0.0117(3)	
W	x	0	0	-0.04762(17)	-0.04827
	y	0.1895(6)	0.18652	0.48387(13)	0.48930
	z	0.25	0.25	0.20900(13)	0.20798
	U_{eq}	0.0047(15)		0.00936(19)	
O1	x	0.2112(15)	0.20969	0.223(3)	0.22598
	y	0.918(4)	0.91069	0.511(3)	0.50807
	z	0.4645(14)	0.45827	0.034(2)	0.03741
	U_{iso}	0.0079(11)		0.008(2)	
O2	x	0.2414(16)	0.24264	-0.150(3)	-0.14766
	y	0.397(5)	0.38919	0.790(3)	0.79670
	z	0.3931(16)	0.39126	0.155(2)	0.14945
	U_{iso}	0.0089(13)		0.012(2)	
O3	x			0.117(3)	0.11768
	y			0.670(3)	0.67751
	z			0.371(2)	0.36775
	U_{iso}			0.010(2)	
O4	x			-0.375(3)	-0.3123
	y			0.457(3)	0.46837
	z			0.300(3)	0.29774
	U_{iso}			0.014(3)	

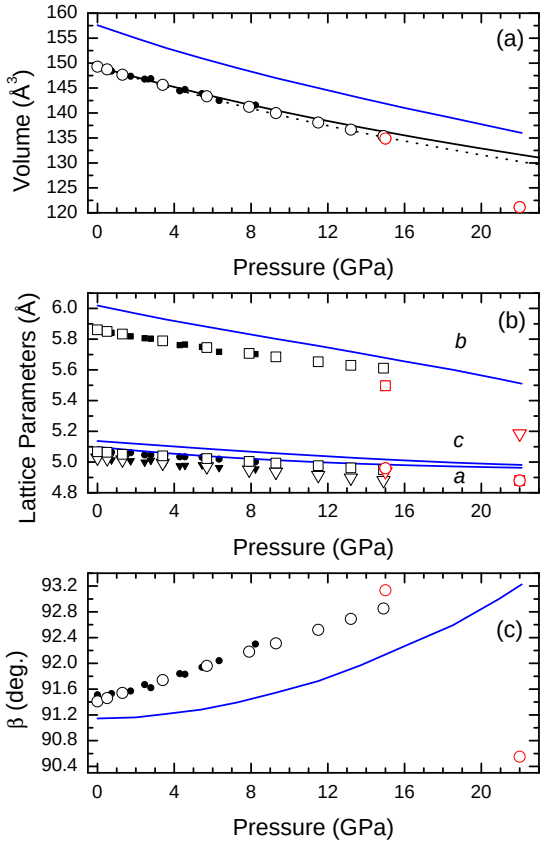

FIG. 5: Pressure dependencies of (a) unit-cell volume, (b) unit-cell axes, and (c) monoclinic β angle of $CdWO_4$. Data shown by solid symbols are from Macavei and Schulz [13] (black) and data shown by black (red) open symbols are from the powder XRD (SXRD) experiment. Fits of the data by Macavei and Schulz [13] and of the data including our powder diffraction data up to 15 GPa to Birch-Murnaghan equations of state (EOS) of second order are drawn by black solid and dashed lines, respectively. At the highest pressure of 22 GPa, only half of the unit-cell volume of the post-wolframite phase is shown to compare with that of the wolframite phase. Lattice parameters at 22 GPa were transformed to those of the respective wolframite cell parameters for comparison. Blue lines represent the calculations.

ganized at the phase transition, which is also expressed in a strong broadening of the single crystal reflections in the high-pressure phase. At the phase transition, the oxygen coordinations of cadmium and tungsten cations are increased from [6] to [6+1] and [7], respectively (Fig. 1).

Our crystal structure solution of the post-wolframite phase of $CdWO_4$ from single-crystal x-ray diffraction clearly contradicts the earlier assumption of the coexistence of two high-pressure phases by Lacomba-Perales et al. [12]. In that work the formation of both a high-pressure phase with a $CuWO_4$-type structure (S. G. $P\bar{1}$) and another one of the scheelite-type (S. G. $I4_1/a$) had been proposed using *ab initio* calculations in order to interpret the experimentally observed Raman modes[12]. Using our experimentally determined crystal structure, the Raman-mode assignment is revisited in section V B and the calculation of the electronic band structure is presented in section V C, where it is discussed with respect to the pressure-induced behavior of the bandgap across the phase transition.

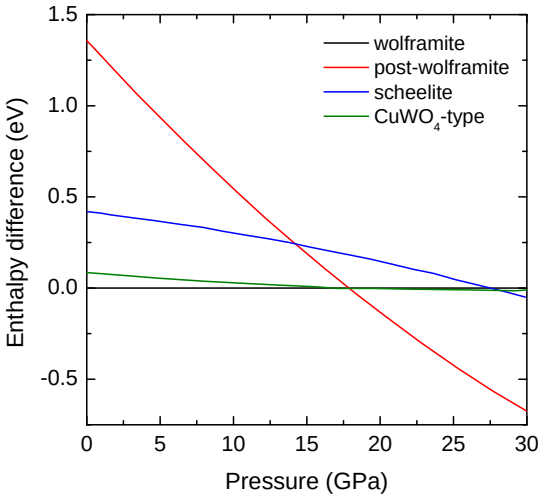

FIG. 6: Calculated enthalpy difference of $CuWO_4$-, scheelite-, and post-wolframite-type phases of $CdWO_4$ with respect to the enthalpy of the low-pressure wolframite-type one. The enthalpy of wolframite is taken as reference.

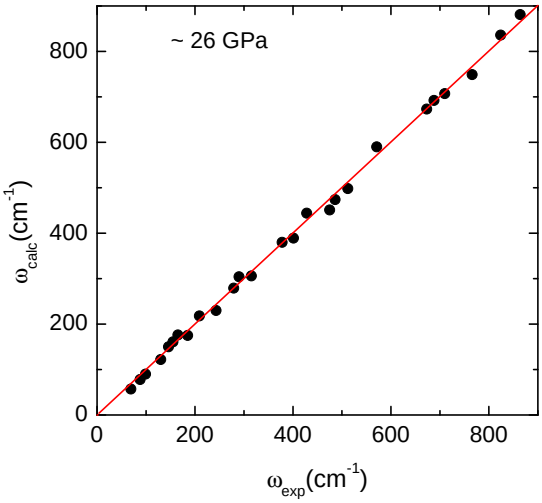

FIG. 7: Calculated Raman mode frequencies (ω_{calc}) represented as a function of the experimentally measured values[12] (ω_{exp}) (black points) to show their linear relation with slope 1 (red line).

V. THEORETICAL RESULTS

A. Phase Stability

The calculated enthalpy differences of $CdWO_4$ for the scheelite-type (S. G. $I4_1/a$), $CuWO_4$-type (S. G. $P\bar{1}$), and post-wolframite phase (S. G. $P2_1/c$) as solved in this study are plotted with respect to the enthalpy of the wolframite-type structure (S. G. $P2/c$) in Fig. 6.

At high pressures, Lacomba-Perales et al. [12] reported from their calculations that the scheelite-type structure would become slightly more stable than the wolframite above 21.2 GPa. This is a pressure slightly higher than that of the phase transition onset (19.5 GPa) observed in the optical absorption study, but can be considered as a reasonable agreement. However, our calculations show that the post-wolframite structure of $CdWO_4$, solved with SXRD at 22 GPa in this work, becomes more stable at 18 GPa than both the wolframite-type structure and the $CuWO_4$-type structure, supporting our experimental structural solution.

In order to obtain the bulk moduli of both low- and high-pressure phases from the calculated data, we have also employed second order Birch-Murnaghan fits for a better comparison with the experimental data. The bulk modulus of the wolframite phase of $CdWO_4$ from the calculations is $B_0 = 111$. This is 9% lower than our updated value using combined experimental data from our study up to 15 GPa and from Macavei and Schulz [13], and 18% lower than the B_0 obtained by Macavei and Schulz [13] up to 8.2 GPa. The bulk modulus obtained in our calculations for the post-wolframite phase it is $B_0 = 114.5$ GPa.

B. Raman modes

Since the previous structural prediction of the post-wolframite phase of $CdWO_4$ had been based on the assignment of experimentally observed Raman modes, we have calculated frequencies and pressure coefficients ($\partial\omega/\partial P$) of the Raman active modes of $CdWO_4$ at 26.1 GPa in the post-wolframite phase. They are presented in Table II together with the experimental values measured with Raman spectroscopy by Lacomba-Perales et al. [12] at 26.9 GPa.

With the point group C_{2h} and $Z = 4$, the post-wolframite structure of $CdWO_4$ (S.G. $P2_1/c$) presents 36 Raman-active modes at zone center $\Gamma = 19A_g + 17B_g$. 26 out of those modes had been experimentally observed[12]. The agreement between the calculated and the experimental frequencies is excellent as can be directly observed in Fig. 7. In respect of the pressure coefficients the calculated and experimental values compare very well for most of the modes if we consider the overlapping and low intensity of many of the Raman modes that were measured in the earlier Raman-spectroscopy study[12]. This confirms that after the phase transition all the observed Raman modes belong to the single high-pressure post-wolframite phase and not to two phases as proposed previously[12].

C. Electronic Structure

Previous calculations had proposed a band crossing in $CdWO_4$ above 10 GPa[10]. However, the experimental data had been limited to 9.9 GPa. In this work we have increased the experimental range to 23 GPa to explore this crossing. As shown in previous works[8,10], the direct band gap of $CdWO_4$ occurs along the Z point of the Brillouin zone. Calculations underestimate the direct band gap of the wolframite phase by 1.11 eV, as expected by DFT-GGA method and predict an-

TABLE II: Calculated and experimental phonon frequencies at ≈ 26 GPa and pressure coefficients of the Raman modes for the high-pressure structure of $CdWO_4$.

	ω_{calc}	$d\omega_{calc}/dP$	ω_{exp}	$d\omega_{exp}/dP$
	(cm^{-1})	(cm^{-1}/GPa^{-1})	(cm^{-1})	(cm^{-1}/GPa^{-1})
symm.	26.1 GPa		26.9 GPa	
A_g	57	2.90	69	1.96
B_g	78	0.43	88	1.94
A_g	90	0.68	99	0.09
B_g	122	0.04	130	0.38
B_g	137	1.42		
A_g	150	-0.49	146	1.35
A_g	161	-0.43	155	0.97
B_g	176	1.97	165	0.19
A_g	178	1.20	185	1.26
B_g	199	1.28		
B_g	218	0.91	209	1.26
A_g	230	-0.77	243	-0.06
A_g	270	2.16		
B_g	279	0.26	279	2.53
A_g	304	2.88	290	0.99
B_g	306	0.19	315	3.00
A_g	354	1.25		
B_g	380	1.46	378	1.65
A_g	389	2.66	401	2.31
B_g	411	3.61		
A_g	444	1.97	428	3.03
B_g	451	1.56	475	2.51
A_g	474	1.90	486	2.72
B_g	498	1.86	512	2.33
B_g	551	2.69		
A_g	558	2.62		
B_g	590	2.43	571	2.62
A_g	656	1.52		
A_g	673	2.39	673	-0.82
A_g	692	2.06	688	2.81
B_g	707	1.71	710	1.60
B_g	727	1.38		
A_g	749	1.50	766	2.12
B_g	803	1.85		
A_g	836	1.43	824	2.23
A_g	881	1.45	864	2.04

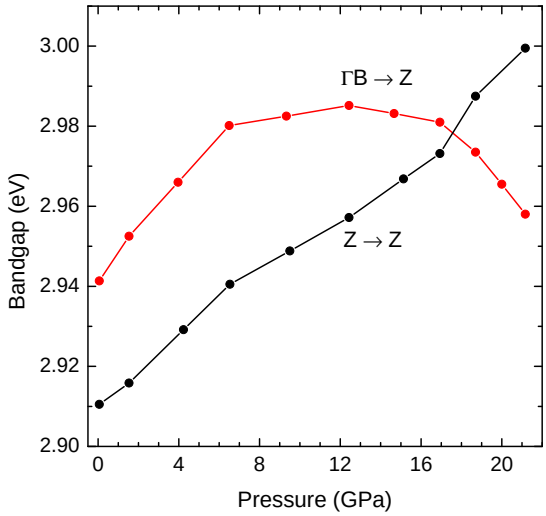

FIG. 8: Calculated pressure dependence of the direct ($Z \rightarrow Z$) and indirect ($\Gamma B \rightarrow Z$) bandgaps of the low-pressure phase of $CdWO_4$.

other indirect band gap $\Gamma B \rightarrow Z$. Ground states are considered to be accurately determined by the DFT-GGA. Since both the direct ($Z \rightarrow Z$) and indirect ($\Gamma B \rightarrow Z$) bandgaps share the same final state we can assume that the underestimation (1.11 eV) is the same for both the direct and indirect transitions. Therefore, at ambient pressure the indirect band gap of $CdWO_4$ should be at around 4.05 eV, 0.03 eV above the direct band gap and therefore, the indirect transition cannot be experimentally observed. As pressure is increased (Fig. 8) the O $2p$ states (which contribute to the valence band[10]) move downwards in energy almost symmetrically at both Z and ΓB points of the Brillouin zone up to 6 GPa. This results in a parallel energy increase of both direct and indirect transitions. Above 6 GPa, the energy of the O $2p$ orbitals continue decreasing at Z but slow down notably at ΓB. Above 12 GPa the energy at ΓB increases. This behavior produces an energy degeneracy of the valence band at both points of the Brillouin zone at 17 GPa. The result is a band crossing of both direct and indirect transitions in agreement with the experimental observation at 16.9 GPa (Fig. 4).

With respect to the high-pressure phase, in Fig. 9 we show the electronic band structure at 18 and 22.8 GPa. Since in the post-wolframite phase there are two additional non-equivalent positions for the O atoms and the formula units per unit cell double from Z = 2 to Z = 4, the number of symmetry directions of the Brillouin zone increases in two points to A and E giving rise to a more complex band structure with respect to the wolframite phase. Regarding the electronic contribution to the valence and conduction bands they are formed by the O $2p$ and the W $5d$ orbitals, respectively, as in the low pressure wolframite phase[10].

In spite of the low dispersion of the bands, as a result of the d electrons, a close inspection to the calculated electronic band structure of the post-wolframite indicates that the maximum of the valence band is located along ΓA and the minimum of the valence band is found along the CY direction of the Brillouin zone. This would result into an indirect

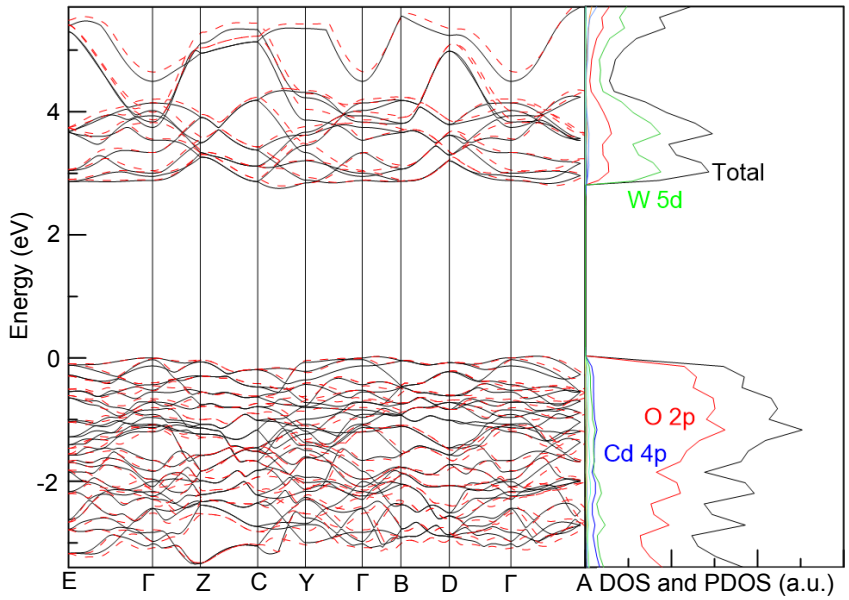

FIG. 9: Electronic-band structure of the post-wolframite phase of $CdWO_4$ at 18 (black) and 22.8 GPa (red). The Fermi level is shown as a dotted line. The right panel shows the corresponding partial and total electron density of states at 18 GPa.

bandgap which would widen with a pressure coefficient of 7.7 meV/GPa as the result of the pressure-induced increase in energy of the conduction band. This value contrasts with the experimental results that indicate a direct bandgap which has a negative pressure coefficient. In fact, the only point of the conduction band that moves downwards in energy with pressure is the point at the ΓA direction of the Brillouin zone. When a direct and an indirect bandgap are very close in energy, usually the direct one is favored. Since the direct transition in ΓA is only 0.1 eV higher in energy than the indirect $\Gamma A \rightarrow CY$, decreases in energy with pressure, and is allowed, we conclude that this direct bandgap is the only one observed experimentally. The calculations underestimate the experimental bandgap in $\sim$1 eV similarly to the understimation of the bandgap of the low-pressure phase.

VI. CONCLUSIONS

The high-pressure post-wolframite structure of $CdWO_4$ has been solved at 22 GPa using single-crystal x-ray diffraction. It is a single phase with monoclinic structure and space group $P2_1/c$. Our result contradicts the previous proposal of two coexisting structures[12]. Density-Functional-Theory based calculations support our structural solution which is more stable than the wolframite-type one above 18 GPa and provides a reliable assignment to the Raman modes observed by Lacomba-Perales et al. [12] for the high-pressure phase. Moreover, optical absorption experiments have been extended to 23 GPa confirming previous results[10] up to 10 GPa. At 16.9 GPa a band crossing of an indirect bandgap previously proposed by electronic band structure calculations[10] within the low-pressure wolframite phase was observed. With regards to the high-pressure phase our optical absorption calculations show a bandgap collapse of 0.7 eV as the result of the phase transition to a direct bandgap of 3.55 eV at 20 GPa. The experimental observation of a strong redshift (-50 meV) of this high-pressure phase bandgap and its direct nature indicate that the calculated indirect $\Gamma A \rightarrow CY$ bandgap in post-wolframite is not experimentally observed and instead a direct bandgap at ΓA appears.

Acknowledgments

J.R.-F. thanks the Juan de la Cierva Program (IJCI-2014-20513) of the Spanish MINECO. A.F. acknowledges financial support from the DFG, Germany, within priority program SPP1236 (Project FR-2491/2-1). W.M. acknowledges the BMBF, Germany (Projects 05K10RFA and 05K13RF1). This paper was partially supported by the Spanish Ministerio de Economıa y Competitividad (MINECO) under grants MAT2013-46649-C04-01/03-P, MAT2016-75586-C4-1/3-P, and No.MAT2015-71070-REDC (MALTA Consolider). Part of this research were carried out at the light source PETRA III at DESY, a member of the Helmholtz Association (HGF). Portions of this work were performed at HP-CAT (Sector 16), Advanced Photon Source (APS), Argonne National Laboratory. HPCAT operations are supported by DOENNSA under Award No. DE-NA0001974 and DOE-BES under Award No. DE-FG02-99ER45775, with partial instrumentation funding by NSF. APS is supported by DOE-BES, under Contract No. DE-AC02-06CH11357.

* Electronic address: javier.ruiz-fuertes@uv.es

[1] S. Rathee, D. Tu, T. T. Monajemi, D. W. Rickey, and B. G. Fallone, Med. Phys. **33**, 1078 (2006).

[2] V. B. Mikhailik and H. Kraus, Phys. Stat. Sol. B **247**, 1583 (2010).

[3] M. M. Silva, S. M. V. Novais, E. S. S. Silva, T. Schmitberger, Z. S. Macedo, and R. F. Bianchi, Mater. Sci. Commun. **136**, 317 (2012).

[4] S. P. Burachas, F. A. Danevich, A. S. Georgadze, H. V. Klapdor-Kleingrothaus, V. V. Kobychev, B. N. Kropivyansky, V. N. Kuts, A. Muller, V. V. Muzalevsky, A. S. Nikolaiko, et al., Nucl. Instrum. and Methods in Phys. Research A **369**, 164 (1996).

[5] F. A. Danevich, A. S. Georgadze, V. V. Kobychev, S. S. Nagorny, A. S. Nikolaiko, O. A. Ponkratenko, V. I. Tretyak, S. Y. Zdesenko, Y. G. Zdesenko, P. G. Bizzeti, et al., Phys. Rev. C **67**, 014310 (2003).

[6] M. Kirm, V. Nagirnyi, E. Feldbach, M. de Grazia, B. Carré, M. Merdji, S. Guizard, G. Geoffroy, J. Gaudin, N. Fedorov, et al., Phys. Rev. B **79**, 233103 (2009).

[7] S. S. Novosad, L. V. Kostyk, I. S. Novosad, A. P. Luchenko, and G. B. Stryganyuk, Acta Phys. Polonica A **122**, 717 (2012).

[8] Y. Abraham, N. A. W. Holzwarth, and R. T. Williams, Phys. Rev. B **62**, 1733 (2000).

[9] M. Fujita, M. Itoh, T. Katagiri, D. Iri, M. Kitaura, and C. B. Mikhailik, Phys. Rev. B **77**, 155118 (2008).

[10] J. Ruiz-Fuertes, S. López-Moreno, J. López-Solano, D. Errandonea, A. Segura, R. Lacomba-Perales, A. Muñoz, S. Radescu, P. Rodríguez-Hernández, M. Gospodinov, et al., Phys. Rev. B **86**, 125202 (2012).

[11] A. Jayaraman, S. Y. Wang, and S. K. Sharma, Current Science **69**, 44 (1995).

[12] R. Lacomba-Perales, D. Errandonea, D. Martínez-García, P. Rodríguez-Hernández, S. Radescu, A. Mújica, A. Muñoz, J. C. Chervin, and A. Polian, Phys. Rev. B **79**, 094105 (2009).

[13] J. Macavei and H. Schulz, Z. Kristallogr. **207**, 193 (1993).

[14] G. E. Jellison Jr., M. A. McGuire, L. A. Boatner, J. D. Budai, E. D. Specht, and D. J. Singh, Phys. Rev. B **84**, 195439 (2011).

[15] H. K. Mao, P. M. Bell, J. W. Shaner, and D. J. Steinberg, J. Appl. Phys. **49**, 3276 (1978).

[16] A. Rothkirch, G. D. Gatta, M. Meyer, S. Merkel, M. Merlini, and H. P. Liermann, J. Synchrotron Rad. **20**, 711 (2013).

[17] Agilent, *Crysalis^{Pro} software system*, version 1.171.36.28, Agilent Technologies UK Ltd., Oxford, UK (2013).

[18] G. M. Sheldrick, Acta Crystallogr. A **64**, 112 (2008).

[19] A. L. Spek, Acta Cryst. D **65**, 148 (2009).

[20] L. J. Farrugia, J. Appl. Crystallogr. **32**, 837 (1999).

[21] P. Hohenberg and W. Kohn, Phys. Rev. **139**, 864 (1996).

[22] G. Kresse and J. Hafner, Phys. Rev. B **47**, 558 (1993).

[23] G. Kresse and J. Hafner, Phys. Rev. B **49**, 14251 (1994).

[24] G. Kresse and J. Furthmüller, Phys. Rev. B **54**, 11169 (1996).

[25] J. Perdew, K. Burke, and M. Ernzerhof, Phys. Rev. Lett. **77**, 3865 (1996).

[26] P. E. Blöch, Phys. Rev. B **50**, 17953 (1994).

[27] G. Kresse and D. Joubert, Phys. Rev. B **59**, 1758 (1999).

[28] H. J. Monkhorst and J. D. Pack, Phys. Rev. B **13**, 5188 (1976).

[29] J. Ruiz-Fuertes, S. López-Moreno, D. Errandonea, J. Pellicer-Porres, R. Lacomba-Perales, A. Segura, P. Rodríguez-Hernández, A. Muñoz, A. H. Romero, and J. González, J. Appl. Phys. **107**, 083506 (2010).

[30] F. Urbach, Phys. Rev. **92**, 1324 (1953).

[31] S. Klotz, J.-C. Chervin, P. Munsch, and G. L. Marchand, J. Phys. D: Appl. Phys. **42**, 075413 (2009).

[32] J. Ruiz-Fuertes, D. Errandonea, F. J. Manjón, D. Martínez-García, A. Segura, V. V. Ursak, and I. M. Tiginyanu, J. Appl. Phys. **103**, 063710 (2008).

[33] D. Errandonea, D. Martínez-García, R. Lacomba-Perales, J. Ruiz-Fuertes, and A. Segura, Appl. Phys. Lett. **89**, 091913 (2006).

[34] R. Lacomba-Perales, D. Errandonea, A. Segura, J. Ruiz-Fuertes, P. Rodríguez-Hernández, S. Radescu, S. López-Moreno, A. Mújica, and A. Muñoz, J. Appl. Phys. **110**, 043703 (2011).

[35] V. Panchal, D. Errandonea, A. Segura, P. Rodríguez-Hernández, A. Muñoz, S. López-Moreno, and M. Bettinelli, J. Appl. Phys. **110**, 043723 (2011).

[36] D. Errandonea, C. Popescu, A. B. Garg, P. Botella, D. Martínez-García, J. Pellicer-Porres, P. Rodríguez-Hernández, A. Muñoz, V. Cuenca-Gotor, and J. A. Sans, Phys. Rev. B **93**, 035204 (2016).

[37] J. Ruiz-Fuertes, A. Friedrich, O. Gomis, D. Errandonea, W. Morgenroth, J. A. Sans, and D. Santamaría-Pérez, Phys. Rev. B **91**, 104109 (2015).